JOURNAL OF GEOPHYSICAL RESEARCH, VOL. 101, NO. B1, PAGES 713–731, JANUARY 10, 1996

Magma ascent simulations of Etna's eruptions aimed at internal system definition

Flavio Dobran[1] and Silvia Coniglio

Global Volcanic and Environmental Systems Simulation, Rome, Italy

Abstract. The internal system of Etna was studied by employing a nonequilibrium two-phase flow model of magma ascent which accounts for different gas-magma flow regimes and gas loss to surrounding conduit fractures when the magma pressure exceeds the local lithostatic pressure. Simulations of different phases of the 1974 and 1989 eruptions of Etna with different flow regimes in conduits suggest that the pyroclastic, strombolian, lava fountaining, and effusive lava flow activity can be modeled by effectively accounting for different physical processes of magma ascent. Results from simulations and geophysical and geological data suggest that magma ascent at Etna may occur along a central conduit or inclined conduits from a magma storage region located from 8 to 9 km below the summit, depending on the regional tectonic stresses and characteristics of the magma supply system. The results also suggest the existence of a structurally weak zone from 1 to 4 km below the summit where magma may accumulate and from which fracture systems and magma ascent with gas loss to fractures may propagate to the eruptive vents at the surface. The predicted excess magmatic pressure over lithostatic in the upper regions of conduits without gas loss to fractures suggests fracturing of the volcanic edifice during initial stages of eruptions and subsequent magma ascent and gas loss along these fractures. Modeling of the changes of activity at Etna requires significant new efforts in geophysics aimed at high-resolution internal system definition.

Introduction

During historical time, most of Etna's activity has been effusive, and most alkali basalt products have erupted from vents outside the summit cone. Etna's eruptive evolution and activity are deeply affected by the regional geodynamic macrosystems, resulting in a complex interaction of tensile and compressive fields responsible for volcanic superficial structures and eruptive cone distributions [*Frazzetta and Villari*, 1981; *Murray*, 1990]. The summit region is dominated by degassing and explosive activity, ranging in style from strombolian to subplinian [*Calvari et al.*, 1991]. An important feature of Etna's activity is the persistence of voluminous summit crater degassing of H_2O, CO_2, and SO_2 [*Allard et al.*, 1991; *Allard*, 1994; *Chester et al.*, 1985].

Effusive, strombolian, and subplinian activity at Etna can occur intermittently and simultaneously at different vents even during a single eruption, reflecting the complexity of its internal system and/or magma supply into the system [*Chester et al.*, 1985; *Hughes et al.*, 1990; *Murray*, 1990]. Recent physical modeling of magma ascent along the volcanic conduits of explosive volcanoes [*Dobran*, 1992; *Papale and Dobran*, 1993, 1994; *Coniglio and Dobran*, 1995] has allowed better constraints on the volcanic eruption parameters obtained from volcanological, petrological, geophysical, and observational data. Moreover, modeling of magma ascent from a magma reservoir to the Earth's surface which allows for changes in magma reservoir pressure, magma composition along the conduit due to gas exsolution, flow regime, and gas loss to fractures can be used to constrain better the internal system of a volcano by comparing the predicted conditions at the vent with field data [*Woods and Koyaguchi*, 1994; *Jaupart and Allègre*, 1991; *Vergniolle and Jaupart*, 1990]. However, an application of such modeling approaches to nonexplosive volcanoes with small eruption rates such as Etna is particularly difficult due to the lack of relevant internal system data, such as the geometry of conduits, physical characteristics of rocks surrounding the conduits, and petrological and geophysical data defining the magma source region.

The purpose of this paper is to present results from computer simulations using different physical models of magma ascent to assess the internal system of Etna. For this purpose, we employed a one-dimensional two-phase flow nonequilibrium thermofluid-dynamic model which accounts for changing magma composition and flow regimes along the conduit as the dissolved magmatic gas exsolves and forms a gas phase, and for the gas loss from the conduit into the surrounding frac-

[1] Also at Department of Earth System Science, New York University, New York.

Paper number 95JB02248.
0148-0227/96/95JB-02248$05.00

tures as the ascending magma pressure exceeds the local lithostatic pressure. Simulations were performed for different phases of the 1974 and 1989 eruptions of Etna which reflect two limiting cases of recent eruptions. The 1974 eruption occurred from a vent located away from the summit region and reflects magma ascent along an eccentric conduit system [*Bottari et al.*, 1976]. The 1989 eruption took place essentially from a crater within the summit cone and reflects magma ascent along the central conduit system of Etna [*Calvari et al.*, 1991]. These recent eruptions of Etna are well documented and reflect better the present state of its internal system than other historical eruptions.

Results from simulations demonstrate that various eruptive styles such as strombolian, lava fountaining, subplinian, and lava effusion during the 1974 and 1989 eruptions may be explained by the rock permeability in the upper regions of the system, different locations of magma storage, tectonic stresses, and ascending magma flow characteristics which govern the opening and closing of different size conduits along different fracture systems. In particular, it is hypothesized that the changes of activity during an eruption can be associated with the internal system relaxation where the presence of rock fractures and the difference between the magmatic and lithostatic pressure control the flow of gas through the subsurface fractures and its release to the atmosphere. The release of gas from magma in the conduit to the surrounding conduit fractures determines the nature of the erupted magma or eruptive activity at the surface. Moreover, results also suggest that magma ascends from a storage region located from 8 to 9 km below the summit and that a structurally weak zone from 1 to 4 km below the summit exists where magma may accumulate and degas.

Geological Setting of Etna and Inferred Internal System

Etna is the largest volcano in Europe. It rises 3300 m above sea level and is located at the northeastern edge of Sicily (Figure 1a). This stratovolcano has a basal diameter of about 40 km and lies between two main geodynamical systems: the Appennine-Maghrebian chain to the north and the Hyblean Maltese foreland to the south (Figure 1b). The complex relative motion of these two systems produces compressive stresses along the north-south direction and tensile stresses along the east-west direction [*Frazzetta and Villari*, 1981; *Fabbri et al.*, 1982; *Lo Giudice et al.*, 1982].

The complex tectonic and structural environment of Etna is also reflected by the substrata under its volcanic cover. *Lentini* [1981] analyzed and classified the sedimentary sequences surrounding Etna based on the present outcrops around the volcano. From geological data and observations he inferred a geological section of the sedimentary piles under Etna which establishes the presence of a discontinuity between the carbonatic basement represented by the Hyblean Plateau and the flysh units related to the northern compressive front represented by the Maghrebian-Appennine chain at a depth of about 6 km below sea level.

The volcanic cover and related eruptive mechanisms had been intensively observed and studied by several authors as described by *Chester et al.* [1985], *Hughes* [1990], and *Murray* [1990]. The thickness of the volcanic cover under the summit is estimated to be about 2 km, where the stratigraphic discontinuity between this cover and the flysch is considered irregular and having a minimum thickness of few hundred meters on the eastern part of the coastline [*Lentini*, 1981]. The volcanic products of Etna consist mainly of aa lavas and subordinate pyroclastic deposits related to the explosive activity. The most frequent explosive activity consists of strombolian eruptions occurring from summit craters and cinder cones dispersed on Etna's flanks. Etna also produced large explosive eruptions which occurred in historical times [*Tanguy*, 1981; *Chester et al.*, 1985].

Physical modeling of magma ascent at Etna requires a knowledge of the conduit geometry and location of magma sources which may be established by using geophysical techniques and analyses. Using a seismic tomography technique, *Hirn et al.* [1991] established the presence of a high-velocity body extending vertically from the summit of Etna to about 6 km depth below sea level and laterally with a diameter of about 10 km. Below this depth, a low-velocity zone of seismic waves was interpreted as due to a possible magma reservoir which correlates with the recognized geodynamical discontinuity between the carbonatic basement of the Hyblean Plateau and the flysch of the Maghrebian-Appennine chain located at the same depth [*Lentini*, 1981]. The great extension of the high-velocity body is probably due to the difficulty of obtaining clear signals to recognize minor bodies at different locations within the volcano. Statistical analyses of shallow earthquakes [*Lo Giudice et al.*, 1982; *Lo Giudice and Rasà*, 1992] also indicate that the eastern portion of Etna has been mostly affected by low seismicity due to the local tensile stress field. By comparing these geophysical data with the geological studies it may be inferred that magma ascent at Etna occurs from a magma source region located at about 8 km below the summit cone. This information, together with relative thicknesses and densities of various strata lying above this depth, was then used in simulations as further discussed below.

Characteristics of 1974 and 1989 Eruptions of Etna

Characteristics of the 1974 Eruption

On January 20, 1974, an intense seismic event caused intermittent strombolian events at the summit of Mount Etna [*Bottari et al.*, 1976]. The subsequent eruptive activity from January 30 to March 29 can be divided into two phases: phase I from January 30 to February 17 and phase II from March 11 to 29.

During the early afternoon of January 30, a new eruptive vent opened at 1670 m above sea level on the west-

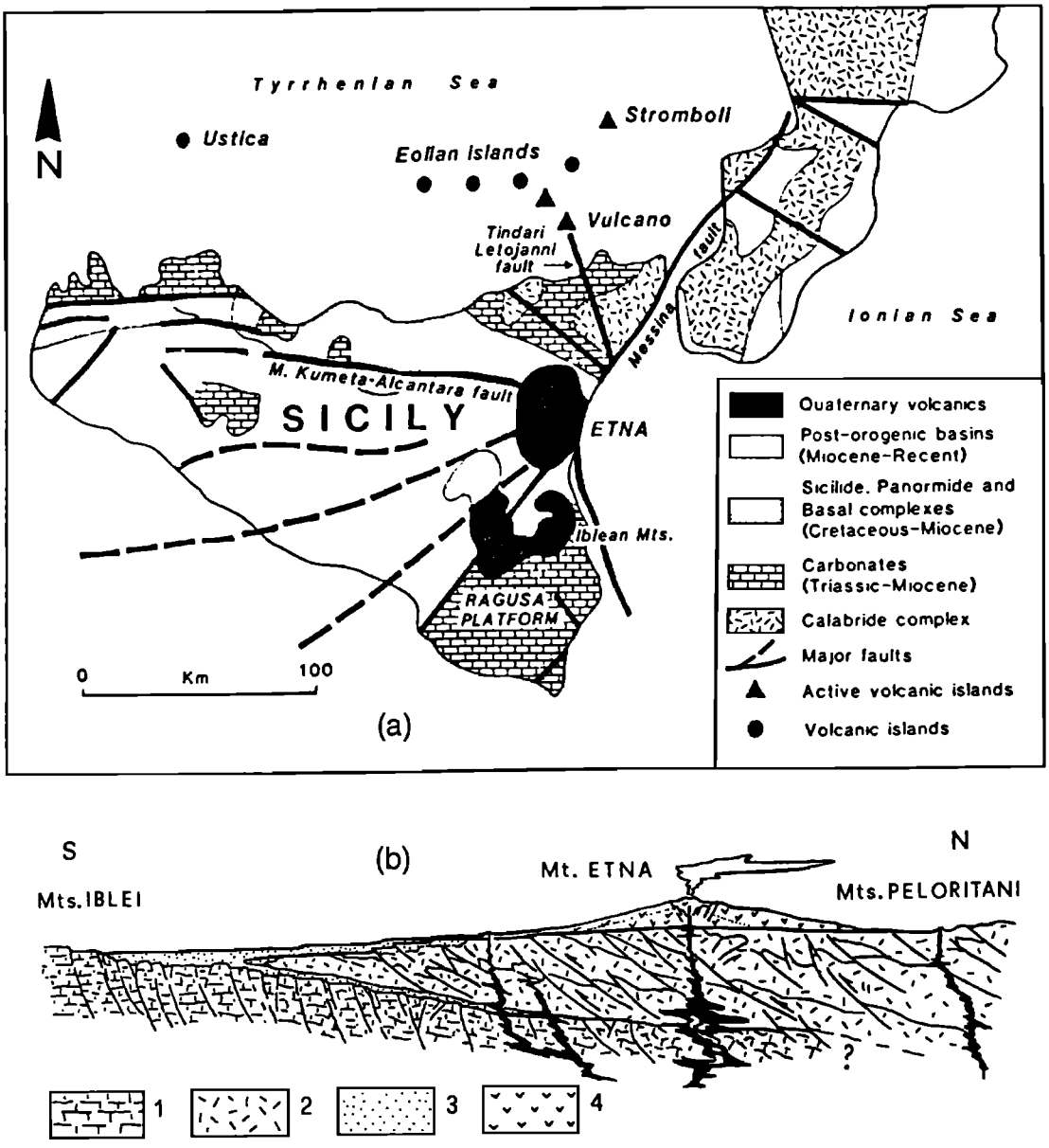

Figure 1. (a) Generalized geologic and tectonic map of Sicily, showing the distribution of volcanic centers [*Grindley*, 1973; *Rittmann*, 1973; *Chester et al.*, 1985]; and (b) schematic section through the Etnean area: 1 Hyblean Plateau, 2 overthrust terrains of the Appennine-Maghrebian chain, 3 Quaternary sediments of the Gela-Catania foredeep, 4 volcanic edifice of Etna [*Lo Giudice and Rasà*, 1992].

ern flank of Etna and displayed intense strombolian activity and lava fountaining. The eruptive activity from this vent built the Monte De Fiore I cone. The effusive activity during the first phase was atypical whereby some effusive vents opened at different times and on different sides of the cone and produced high-viscosity lava flows of short lengths [*Guest et al.*, 1974]. This effusive activity took place contemporaneously with the explosive activity which caused an irregular formation of the cone. On February 12, the violent and intermittent strombolian activity decreased, and on February 17 it ended. During this time, the activity at the summit craters was characterized by emissions of gas and ash. The pyroclastic and lava flow activity of phase I produced a mean eruption rate of 401×10^3 m^3/d or 0.123×10^5 kg/s [*Bottari et al.*, 1976].

On February 26 a new seismic crisis started, and on March 11, phase II activity began. This produced the opening of an eruptive vent at 1650 m above sea level, situated 200 m west of Monte De Fiore I. During this time, the summit craters exhibited violent emissions of gas and ash. The strombolian activity reached a climax on March 12 and subsequently decreased until the end of the eruption. This activity produced a new small cone Monte De Fiore II and only one effusive vent on the western side of the cone and three lava flows of smaller viscosity than of the phase I eruption. The activity at the summit craters was similar to that of phase I

but in addition produced some strombolian events. The pyroclastic and lava flow activity of phase II produced a mean eruption rate of 292×10^3 m^3/d or 0.896×10^4 kg/s [*Bottari et al.*, 1976].

Characteristics of the 1989 Eruption

In the summer of 1989, the central craters (Bocca Nuova, North-East Crater, South-East Crater, and Voragine) displayed strombolian and degassing activity. From the end of August until the early days of September, this activity increased at the Voragine and South-East Crater. Voragine produced a 2-km-high tephra column with internal lava fountaining for less than an hour, and the South-East Crater displayed an increase in activity on September 10. The subsequent activity from September 11 to October 9 can be divided into two phases: phase I from September 11 to 23 and phase II from September 27 to October 9 [*Bertagnini et al.*, 1989; *Calvari et al.*, 1991].

In the morning of September 11, the strombolian activity at the South-East Crater changed into lava fountaining several hundred meters high, with the crater filling with lava and spilling over to the south and producing two lava flows. Significant new activity resumed in the late afternoon which produced a lava pond and strombolian explosions. During the evening hours, lava fountains several hundred meters high were observed again at the South-East Crater with lava overflowing from the crater rim. On September 12, the strombolian activity increased, and by the early morning of September 13, lava overflowed the crater rim. By 0900 hours on the same day, a lava wall up to 800 m high and occupying the entire crater of about 150 m in diameter was observed. This event, lasting for several minutes, produced magma fragmentation in the fountain and an eruptive column about 2 km high. The paroxysmal event at the South-East Crater ended with internal collapses, and after several hours the strombolian activity, lava fountaining, and lava overflow from the crater resumed and by the end of the day left the crater with strombolian explosions. The explosive activity at the North-East Crater, Voragine, Bocca Nuova, and South-East Crater continued during the subsequent days. From September 19 to 23, the South-East Crater produced intermittent strombolian activity, pulsating lava fountaining, paroxysmal events, and several lava flows.

The paroxysmal event of September 13 produced about 2.4×10^6 m^3 of material, lasted for about 10 min, and thus had an eruption rate of about 7×10^6 kg/s [*Calvari et al.*, 1991]. This event will be referred to as phase Ia of the 1989 eruption. The entire period from September 11 to 23 involving (mixed) strombolian, lava fountaining, and lava overflow from the South-East Crater produced about 8.8×10^6 m^3 of lava and an eruption rate of about 0.55×10^6 kg/s [*Bertagnini et al.*, 1989; M. Coltelli, personal communication, 1994]. This event will be referred to as phase Ib of the 1989 eruption.

During phase II of the 1989 eruption, intense strombolian activity in the morning of September 24 at the South-East Crater accompanied the opening of eruptive fractures toward northeast and southeast. The latter fracture produced a wall of lava fountain and lava flow in Valle del Bove. During the following days, the strombolian, lava flow, and degassing activity continued from the South-East Crater. On September 27, the northern fracture produced at the South-East Crater propagated toward Valle del Leone in the east, and the southern fracture propagated toward the south. This produced several eruptive vents and degassed lava flows inside Valle del Leone. Successively, the opening fractures also produced lava flows from new eruptive fissures in Valle del Bove. On October 9, the lava flows stopped and the eruption ended. The lava flow in Valle del Leone produced 26.2 m^3 of lava and a mean effusion rate of 0.65×10^5 kg/s [*Bertagnini et al.*, 1989].

Magma Ascent Modeling

Modeling Approaches

Dobran [1992] developed a nonequilibrium two-phase flow model of magma ascent in volcanic conduits. This model describes a quasi-steady state and one-dimensional flow of magma from a magma reservoir to the surface (Figure 2). The flow of magma in the conduit is assumed to be isothermal, and no heat and mass transfer from magma to the surrounding rocks are allowed. The ascending magma decompresses and begins to exsolve the dissolved gas at a height z_s above the reservoir. Above z_s, the gas bubbles grow by the exsolution of dissolved gas and decompression until the bubble packing becomes so great that the magma flow between the bubbles becomes impeded. This occurs at a gas volumetric fraction of about 0.75 causing the magma to fragment at $z = z_f$. For $z > z_f$, the flow regime consists of a two-phase particle/droplet flow where the fragmented magma particles/drops (or pyroclasts) are entrained in a continuous gas phase. The thermofluid-dynamic model allows for the variation of density and viscosity of magma with the dissolved water content and was subsequently refined by *Papale and Dobran* [1993] by accounting more precisely for this variation with the magma composition. The thermal equilibrium assumption between magma and gas is justified by the very large thermal capacity of magma, short transit time through the conduit, and absence of magma-water interaction [*Dobran*, 1992] which appear justifiable for modeling magma ascent along the conduits at Etna.

The assumption of no mass transfer from the conduit to the surrounding rocks must be, however, carefully evaluated for a volcano such as Etna. This volcano has low eruption rates, and a large quantity of gas may be absorbed by fractures within the system, causing significant changes of flow regimes in the conduits and activity on the surface. Moreover, the assumption in the model of a single bubbly flow regime from the gas

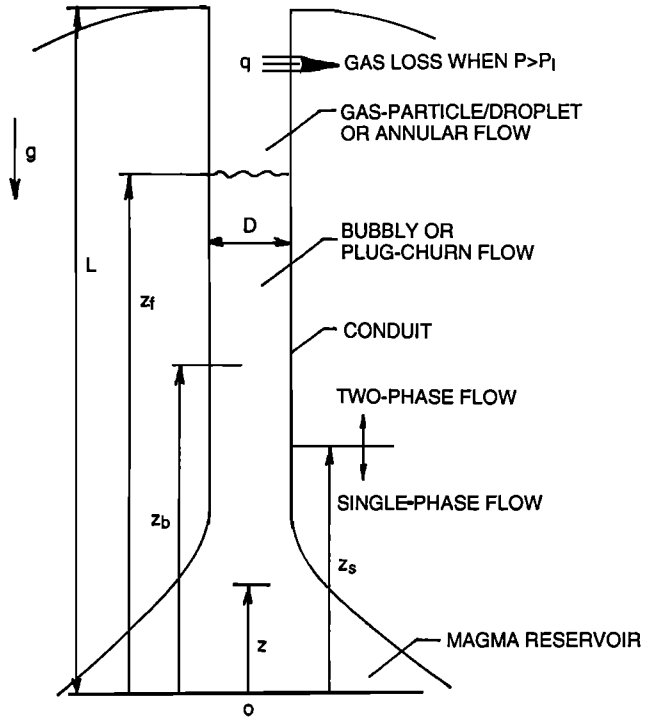

Figure 2. Illustration of a volcanic conduit of length L and diameter D. Magma is accelerated from the magma reservoir at z=0, begins exsolving at a height z_s, and may change from the bubbly to the churn turbulent flow regime at a height z_b. The bubbly flow regime fragments and changes to the particle/droplet flow, or the churn turbulent flow changes to the annular flow, at a height z_f. Gas loss from the conduit is allowed when the magma pressure exceeds the local lithostatic pressure.

exsolution level to the magma fragmentation level must also be reevaluated, since it is well known that the flow of a low viscosity liquid and gas produces several flow regime changes along a conduit [*Wallis*, 1969]. Such a two-phase flow involves a bubbly flow regime for gas volumetric fractions below about 0.3, a plug-churn flow regime for volumetric fractions between about 0.3 and 0.8, and an annular flow regime above the gas fraction of about 0.8. In the plug-churn flow regime, the bubbles coalesce into large bubbles, and the gas and liquid intermittently move through the conduit. When these bubbles become large, or the flow regime transforms to the annular flow, the gas flows through the core of the tube and liquid along its walls with different velocities, and no fragmentation of magma should occur. For very high viscosity magmas, such as dacites and rhyolites, the plug-churn and annular flow regimes do not appear to exist, since the large drag between the phases tends to impede bubble coalescence and relative motion. However, a basaltic volcano such as Etna with significant tectonic stresses which may limit the conduit geometry during magma ascent may impede magma fragmentation by favoring bubble coalescence within the conduits and thus the establishment of bubbly, plug-churn, or annular flow regimes which permit considerable disequilibrium between the phases.

Initial application of the bubbly-particle/droplet flow model of *Dobran* [1992] to magma ascent at Etna produced vent conditions which were found to be inconsistent with most of the activity of the 1974 and 1989 eruptions of this volcano. Consequently, we revised the above model by allowing for different flow regimes in conduits as well as for the loss of gas from magma to the surrounding fractures when the magma pressure exceeds the lithostatic pressure.

The physical modeling approach of *Dobran* [1992] for the transport of magma from a magma reservoir to the Earth's surface through a volcanic conduit of length L and diameter D (Figure 2) involves conservation of mass and balance of momentum of magma and gas. Below the gas exsolution level $z \leq z_s$ the pressure distribution is governed by the generalized Bernoulli equation

$$P_0 = P + (1+K)\frac{G^2}{2\rho_L} + 4z\frac{f_F}{D}\frac{G^2}{2\rho_L} + \rho_L z g\cos\theta, \quad (1)$$

where P is the pressure, ρ_L is the effective density of magma, G is the mass flowrate per unit area, f_F is a friction loss coefficient, θ is the angle of inclination of the conduit with respect to the vertical, and the subscript zero indicates the magma reservoir conditions. In (1), K is the conduit entrance loss coefficient [*Dobran*, 1992], and the friction coefficient f_F is given by

$$f_F = \frac{16}{Re} + 0.01, \qquad Re = \frac{GD}{\mu_L}, \quad (2)$$

where μ_L is the magma plus crystals viscosity. The magma reservoir pressure P_0 is bracketed by the lithostatic pressure of the overlying rocks and the rock yield stress, it does not depend on the inclination angle of the conduit, and it is determined from the actual stratigraphy of a volcano, i.e.,

$$P_0 = \int_0^L \rho_c g dz + P_{atm} \pm \tau_{yield}, \quad (3)$$

where ρ_c is the local density of the country rock and τ_{yield} is the rock yield stress which ranges from 1 to 10 MPa [*Touloukian et al.*, 1981]. In the present work we have assumed, however, that P_0 depends only on the lithostatic pressure.

In the two-phase flow region of the conduit (Figure 2), the flow of magma and gas is modeled by the conservation of mass and balance of momentum equations of the two phases separately. Thus

$$\frac{d}{dz}(M_G + M_{Gd}) = -\pi D q \quad (4)$$

$$\frac{d}{dz}(M_L - M_{Gd}) = 0 \quad (5)$$

$$\rho_G u_G A\alpha\frac{du_G}{dz} = -\alpha A\frac{dP}{dz} - F_{LG}A - F_{wG}A - \rho_G \alpha A g\cos\theta \quad (6)$$

$$\rho_L u_L A(1-\alpha)\frac{du_L}{dz} = -(1-\alpha)A\frac{dP}{dz} + F_{LG}A - F_{wL}A - \rho_L(1-\alpha)Ag\cos\theta \quad (7)$$

where the exsolved and dissolved gas mass flow rates, M_G and M_{Gd}, and the liquid magma plus crystals mass flow rate, M_L, are given by

$$M_G = \rho_G \alpha A u_G = XM \quad (8)$$

$$M_{Gd} = Y(1-X)M \quad (9)$$

$$M_L = \rho_L(1-\alpha)Au_L = (1-X)M. \quad (10)$$

In (4)-(10), M is the local mass flowrate in the conduit, u is the velocity, α is the gas volumetric fraction, X is the exsolved gas mass fraction, Y is the dissolved gas mass fraction in the magma, and the subscripts G and L pertain to the gas and magma, respectively. With this notation, the gas component is water vapor and the liquid is magma before magma fragmentation and liquid drops of magma or particles (pyroclasts) after magma fragments.

The gas mass transfer across the conduit wall per unit tube periphery q can be physically modeled by accounting for the surrounding rock permeability and lithostatic pressure and to a good approximation can be determined from the Darcy's law [*Jaupart and Allègre*, 1991], i.e.,

$$q = \rho_G \alpha k(P - P_l), \qquad k \approx \frac{2K'}{\mu_G D}, \quad (11)$$

where K' is the permeability of the surrounding conduit rocks. The local lithostatic pressure P_l does not depend on the inclination angle of the conduit and is determined from

$$P_l = \int_z^L \rho_c g dz + P_{atm}. \quad (12)$$

In the momentum equations (6) and (7), the viscous drag between the gas and conduit wall F_{wG}, the magma and conduit wall F_{wL}, and the gas and magma F_{LG} depend on the flow regime, and for the bubbly, plug-churn, particle/droplet, and annular flows are determined as described by *Dobran* [1987, 1992] and will not be reproduced here. These constitutive equations depend on the density and viscosity of gas and magma which are determined from the density, viscosity, and gas exsolution modeling approach of *Papale and Dobran* [1993].

The differential equations (4)-(7) were solved by an accurate numerical solver as described by *Dobran* [1992] for choked and nonchoked flow conditions at the conduit exit where a choked flow corresponds to the speed of sound of the gas-particle mixture. In this model and subsequent discussion, the flow conditions at the conduit exit must be interpreted as those of the vent, since the effect of a crater above the vent is not modeled. The choked flow condition corresponding to a specified mass eruption rate establishes the vent conditions (pressure, volumetric fraction, gas and magma velocities) and a minimum conduit diameter. For the nonchoked flow conditions at the conduit exit, the atmospheric disturbances are allowed to propagate inside the conduit and it is necessary to specify the conduit diameter and pressure at the exit, where this pressure may correspond to an atmospheric pressure or an overpressure determined, for example, from the weight of lava in a crater above the vent. For the case of gas loss to fractures, only the nonchoked flow conditions at the conduit exit are determined. The computer programs using the above magma ascent modeling approaches which account for different combinations of two-phase flow regimes within the volcanic conduits and gas loss to fractures are described by *Dobran* [1994].

Input Data for Simulations

The magma ascent models described above require input parameters which are extensively documented by *Dobran* [1992], *Dobran and Papale* [1992], *Papale and Dobran* [1993, 1994], and *Coniglio and Dobran* [1995], and some new modifications involving different flow regimes and gas loss to fractures are described by *Dobran* [1994]. Essentially, they consist of the anhydrous composition and physical properties of magma, magma flow rate, conduit length, magma reservoir pressure, local stratigraphy, surrounding rock permeability, and conditions described at the vent. The vent conditions may involve a fixed pressure or choked flow. The former may be used for studying the discharge of magma to the atmosphere under balanced or unbalanced pressure conditions with the atmosphere, whereas the choked flow condition implies that the atmospheric conditions outside of the vent do not affect the flow in the conduit. Tables 1 and 2 summarize the input data for magma ascent modeling and are briefly discussed below.

Magma composition. Data on the chemistry of Etna's lavas which are compiled in many reports of the Istituto Internazionale di Vulcanologia in Catania show only slight differences in important oxide concentrations. For this reason, we performed the simulations

Table 1. Anhydrous Composition of Erupting Magma at Etna

Composition	Average
SiO_2	47.20
TiO_2	1.70
Al_2O_3	17.76
Fe_2O_3	3.78
FeO	6.55
MnO	0.18
MgO	6.21
CaO	10.38
Na_2O	3.32
K_2O	1.80

M. Pompilio (personal communication, 1993), as cited by *Dobran* [1995].

Table 2. Input Parameters for Magma Ascent Modeling for the 1974 and 1989 Eruptions of Etna

Eruption	1974, Phase I	1974, Phase II	1989, Phase Ia	1989, Phase Ib	1989, Phase II
L, km	8.3-9.3	8.3-9.3	8.3-9.3	8.3-9.3	8.3-9.3
P_0, MPa,	181-222	181-222	181-222	181-222	181-222
T, K	1373-1393	1373-1393	1373-1393	1373-1393	1373-1393
ϕ, vol %	10-30	10-30	10-30	10-30	10-30
d_p, μm	200	200	200	200	200
K', m^2	-	10^{-8}-10^{-14}	-	-	10^{-8}-10^{-14}
Y_0, wt %	1-3	1-3	1-3	1-3	1-3
M, kg/s	0.123×10^5	0.896×10^4	7×10^6	0.55×10^6	0.65×10^5

These parameters consist of magma composition (Table 1), conduit length L, magma reservoir pressure P_0, magma temperature T, crystal volumetric fraction ϕ, pyroclasts or particle diameter d_p, rock permeability K', maximum dissolved water content in magma Y_0, and mass eruption rate M.

using only an average composition as reported in Table 1.

Conduit length. Magma supply to the summit of Etna is considered to take place along a central conduit and along subvertical dykes emanating from this conduit which is connected to a feeding system at a depth of about 20 km [*Chester et al.*, 1985]. Seismic data show no evidence of a magma chamber below Etna, but the low velocity data of *Hirn et al.* [1991] suggest that at about 6 km below sea level there may be a possible magma storage region of limited extent. This hypothesis is also confirmed by the work of *Lentini* [1981] who studied the implications of sedimentary substrata on the geodynamics of Etna and suggested that at about 6 km below sea level the flysh of the sedimentary folds contacts the carbonatic basement. For the 1989 eruption taking place essentially from the South-East Crater, we assumed a vertical conduit of uniform diameter, whereas for the 1974 eccentric vent eruption we assumed a constant diameter and an inclined conduit at 45°. It should be noted, however, that at greater depths the conduit may have the form of a fissure and that it could be modeled as such if its dimensions were known. Moreover, the effect of the inclined conduit is to reduce the body force acting on magma. Based on the data uncertainty, the conduit length or location of magma source below the summit of the volcano for both eruptions was parametrized from 8.3 to 9.3 km.

Magma reservoir pressure. The location of magma source and density of overlying rocks determine the magma reservoir pressure (Equation (3)). By collecting the observational and geophysical data and comparing them with the general geophysical knowledge of rock densities and seismic wave velocities, we established this pressure by parametrizing the densities of different stratigraphic layers of the volcano. The uppermost layer with a thickness of 2100 m, the middle layer with a thickness of 3200 m, and the lower layer thickness were thus parametrized with densities of 2200, 2400, 2600, and 2000, 2200, 2400 kg/m^3, which produced pressures of 197.2 and 181 MPa, respectively, for the conduit length of 8.3 km.

Magma temperature. The value of 1373 K for the selected magma temperature can be considered as an average obtained from the thermal data of Etna's lavas [*Pinkerton and Sparks*, 1976] and thermal equilibrium of mineralogical phases [*Trigila et al.*, 1990]. Nevertheless, to reflect a possible variation of this temperature during magma ascent we parametrized this parameter from 1373 to 1393 K.

Crystal content. Modal analyses of lavas pertaining to recent eruptions of Etna are compiled in many reports of the Istituto Internazionale di Vulcanologia (see database references of *Dobran* [1995]). The recorded crystal volumetric fractions reach 30 vol % and may also be representative of crystal fractions during magma ascent [*Armienti et al.*, 1994b]. For this purpose, we parametrized this parameter from 10 to 30 vol %, where 10 vol % is representative for olivine and clinopyroxene phases and 30 vol % is representative for the presence of the plagioclase phase in magma.

Particle diameter. A particle size of d_p=200 μm after magma fragmentation is suggested by the granulometric studies of pyroclastic flow and ash cloud deposits of Mount St. Helens eruption in 1980 which give a median size between 300 to 600 μm for the former and between 39 to 68 μm for the latter [*Kuntz et al.*, 1981]. The above value of particle size was also found to be appropriate for magma ascent modeling at Vesuvius and Mount St. Helens [*Papale and Dobran*, 1993, 1994] but may not be applicable to basaltic magmas such as Etna. Fragmentation of such magmas may produce large-size pyroclasts where they affect the distribution of gas and pyroclasts velocities along the conduit but do not significantly affect the flow characteristics at the vent [*Dobran*, 1992].

Rock permeability. Permeabilities of rocks surrounding the volcanic conduits may range from about 10^{-6} to 10^{-16} m^2 [*Heiken et al.*, 1988; *Jaupart and Allègre*, 1991]. The lower value corresponds to a highly fractured rock, whereas the upper limit is representative of hydrothermal circulation systems. Gas loss to fractures is highly dependent on the surrounding rock permeability, and consequently, we performed a parametric study using permeabilities from 10^{-8} to 10^{-14} m^2 which correspond to maximum fracture dimensions of less than a centimeter per meter of rock.

Dissolved water content. Data of the dissolved water content of Etna's magmas derive mainly from fluid inclusion studies. *Metrich and Clocchiatti* [1989]

found water contents exceeding 3 wt % of a wide variety of lava samples pertaining to the historical eruptions of Etna, whereas recenty *Armienti et al.* [1994a] established that this content is around 2 wt %. To reflect the uncertainty in the maximum dissolved water content in magma, we carried out a parametric study involving water contents from 1 to 3 wt %.

Mass eruption rate. As discussed above, different phases of the 1974 and 1989 eruptions involve different mass eruption rates derived from the volumes of pyroclasts and lavas, average density of lavas of 2650 kg/m^3, and times associated with the eruptive phases. For the 1974 eruption, we used a mean mass eruption rate of 0.123×10^5 kg/s for phase I lasting from January 30 to February 17, and a mean value of 0.896×10^4 kg/s for phase II lasting from March 11 to 29. During the 1989 eruption, the maximum mass eruption rate of 7×10^6 kg/s occurred on September 13 (phase Ia), whereas the mean eruption rate from September 11 to 23 corresponds to 0.55×10^6 kg/s (phase Ib). The mean eruption rate for phase II corresponds to 0.65×10^5 kg/s. The uncertainty in the above data was estimated to be about ±30% (S. Calvari, personal communication, 1994). Eruption times pertaining to different phases of 1974 and 1989 eruptions are much greater than the times associated with magma ascent which justifies a quasi steady state assumption in modeling. Moreover, each phase of the eruption is intermittent but could not be split further at present due to the lack of geological and geophysical data.

Results

The results presented in this section pertain to simulations of different phases of the 1989 and 1974 eruptions of Etna. These simulations were performed for the range of parameters summarized in Tables 1 and 2, and only the most significant results will be presented. The range of uncertainties in input parameters related to the properties of magma was reduced by performing a parametric study. Results showed that the dissolved water content of 2 wt % gives more reliable conduit exit conditions (such as pressure, velocities, and gas volumetric fractions) when confronted with field observations pertaining to the studied eruptions and that a slight variation of magma temperature from 1373 K does not produce any significant variation of numerical results. Moreover, the crystal content variation from 10 to 30 vol % for dissolved water contents from 1 to 3 wt % did not produce any significant changes in results and we subsequently employed the value of 10 vol %. Simulations were carried out for three different flow conditions in the conduit. The bubbly flow (BF) simulations employed a bubbly flow in the conduit from the onset of gas exsolution at $z=z_s$ ($\alpha=0$) until magma fragmentation at $z=z_f$ ($\alpha=0.75$) with subsequent change to the gas-particle/droplet flow (Figure 2). The plug-churn flow (PCF) simulations were performed by assuming a bubbly flow from $z=z_s$ to $z=z_b$ ($\alpha=0.3$), churn turbulent flow from $z > z_b$ to $z=z_f$ ($\alpha=0.75$), and annular flow for $z > z_f$. The gas loss (GL) simulations employed

Table 3. Simulations Discussed of Different Phases of the 1989 and 1974 Eruptions of Etna

Case	Eruption Phase	Flow Regime	Flow Condition	P_0 MPa	L km	$g\cos\theta$ m/s^2	M kg/s	D m	K' m^2
1	1989Ia	BF	CH	197.2	8.3	9.81	7×10^6	19.2	-
2	1989Ia	BF	CH	181	8.3	9.81	7×10^6	25.5	-
3	1989Ia	PCA	CH	197.2	8.3	9.81	7×10^6	17.1	-
4	1989Ia	BF	CH	222.7	9.3	9.81	7×10^6	20.3	-
5	1989Ib	BF	CH	197.2	8.3	9.81	0.55×10^6	6.3	-
6	1989Ib	PCA	CH	197.2	8.3	9.81	0.55×10^6	7.1	-
7	1989Ib	BF	CH	181	8.3	9.81	0.55×10^6	8.1	-
8	1989Ib	PCA	CH	181	8.3	9.81	0.55×10^6	11.8	-
9	1989II	PCA	CH	197.2	8.3	9.81	0.65×10^5	3.8	-
10	1989II	PCA	CH	181	8.3	9.81	0.65×10^5	6.7	-
11	1989II	GL	-	197.2	8.3	9.81	0.65×10^5	5	10^{-8}
12	1989II	GL	-	197.2	8.3	9.81	0.65×10^5	5	10^{-12}
13	1989II	GL	-	197.2	8.3	9.81	0.65×10^5	5	10^{-13}
14	1989II	GL	-	197.2	8.3	9.81	0.65×10^5	10	10^{-8}
15	1974I	BF	CH	197.2	8.3	6.93	0.123×10^5	1.3	-
16	1974I	PCA	CH	197.2	8.3	6.93	0.123×10^5	1.9	-
17	1974II	BF	CH	197.2	8.3	6.93	0.896×10^4	1.17	-
18	1974II	PCA	CH	197.2	8.3	6.93	0.896×10^4	1.76	-
19	1974II	GL	-	197.2	8.3	6.93	0.896×10^4	2	10^{-9}
20	1974II	GL	-	197.2	8.3	6.93	0.896×10^4	2	10^{-12}
21	1974II	GL	-	197.2	8.3	6.93	0.896×10^4	2	10^{-13}
22	1974II	GL	-	197.2	8.3	6.93	0.896×10^4	2	10^{-14}
23	1974II	GL	-	197.2	8.3	6.93	0.896×10^4	10	10^{-9}

CH, choked flow; BF, bubbly-particle/droplet flow; PCA, bubbly-plug-churn-annular flow; GL, gas loss to fractures. T=1373 K, ϕ=0.1, d_p=200 μm, Y_0=2 wt %.

bubbly flow and gas loss to fractures for $P \geq P_l$. Table 3 summarizes the simulations discussed in the paper.

The September 13 explosive phase of the 1989 eruption which produced a 2-km-high sustained eruption column with magma fragmentation (phase Ia) was simulated with BF and PCA flow regimes. Figure 3 shows choked BF results pertaining to P_0=197.2 and 181 MPa, with all other parameters being the same (cases 1 and 2 in Table 3). A larger magma reservoir pressure produces a conduit diameter of 19.2 m, whereas a smaller pressure produces a diameter of 25.5 m. A magma reservoir pressure of 197.2 MPa produces 17.7 MPa of pressure difference between the lithostatic and magmatic pressures at the magma fragmentation depth of about 600 m, whereas the corresponding pressure and depth for P_0=181 MPa are 25.3 MPa and 1100 m, respectively. It is important to note that the largest difference between the magmatic and lithostatic pressures occurs over a significant portion of the conduit, from about 1 to 4 km below the vent for both magma reservoir pressures. A larger magma reservoir pressure also produces a larger vent exit pressure (2.1 versus 1.1 MPa), a smaller gas volumetric fraction, and comparable gas and pyroclast velocities (about 120 m/s). Choked PCA flow regimes (case 3 in Table 3) produce a conduit diameter of about 17 m and vent gas and magma velocities of about 500 and 45 m/s, respectively, gas volumetric fraction of about 0.75, and pressure of about 0.6 MPa. The effect of maintaining the same stratigraphy as for the case of magma reservoir pressure of 197.2 MPa but by increasing the conduit length from 8.3 to 9.3 km (case 4 in Table 3) produces a conduit diameter of 20.3 m, 17.8 MPa of pressure difference between the magmatic and lithostatic pressures at the magma fragmentation level located at about 650 m below the surface, a vent exit pressure of about 1 MPa, and comparable vent velocities and gas volumetric fraction as in cases 1 and 2.

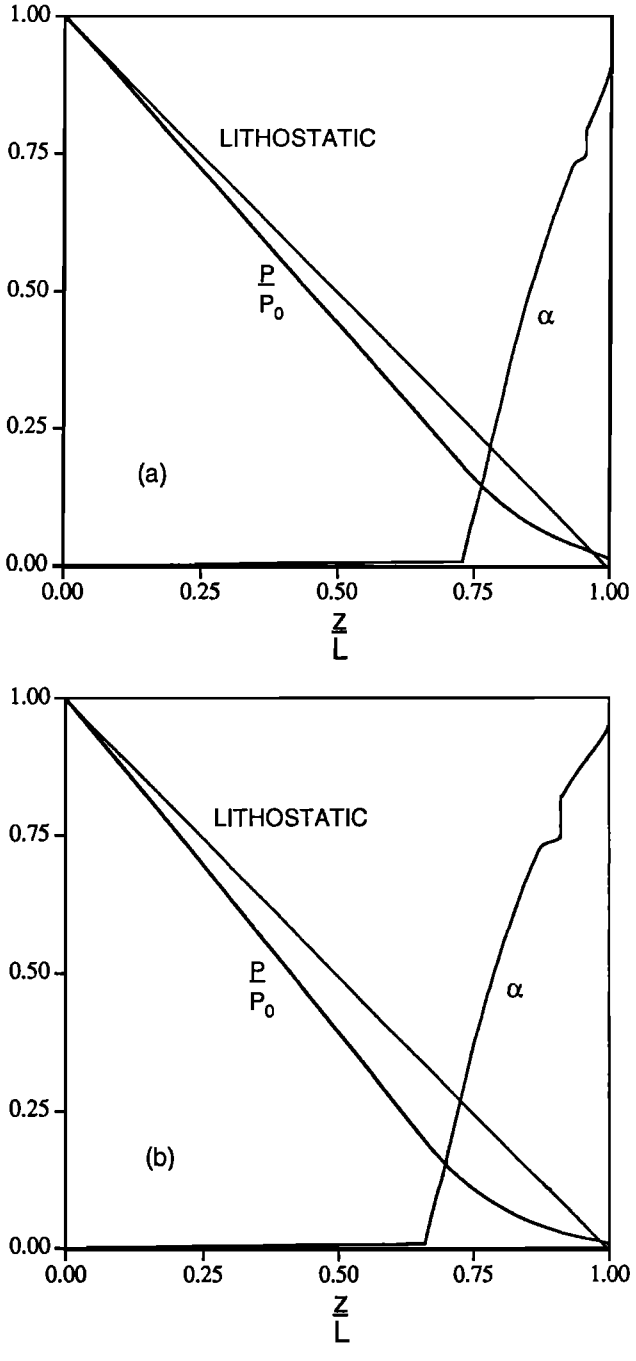

Figure 3. Nondimensional pressure and gas volumetric fraction variations along the conduit corresponding to BF cases 1 and 2 in Table 3 (phase Ia of the 1989 eruption). (a) P_0=197.2 MPa and (b) P_0=181 MPa, with all other parameters being the same.

The strombolian, lava fountaining, and lava overflow activity from the South-East Crater from September 11 to 23 (phase Ib) was simulated with BF, PCA, and GL flow regimes. Figure 4 illustrates the pressure and gas volumetric fraction distributions along the conduit for cases 5 and 6 in Table 3 corresponding to the choked flow conditions. BF flow regimes (case 5) produce a conduit diameter of about 6 m, magma fragmentation at about 660 m below the vent, and vent pressure of about 1.5 MPa, velocities of about 120 m/s, and gas volumetric fraction of about 0.94. PCA flow regimes (case 6) produce a conduit diameter of about 7 m, change of the churn turbulent to the annular flow regime at about 750 m below the vent, and vent pressure of about 0.3 MPa, gas and magma velocities of about 500 and 15 m/s, respectively, and a gas volumetric fraction of about 0.75. BF flow regimes produce a higher vent pressure and gas volumetric fraction than PCA flow regimes, whereas the gas and magma velocities show opposite trends. These trends are more clearly seen in Figures 5 and 6 which illustrate the variation of pressure and gas and magma velocities at the vent for different diameter conduits and magma reservoir pressures. As seen from Figures 5 and 6, the choked flow condition produces minimum diameters and highest velocities at the vent, and exit pressures which are quite low but usually higher than the atmospheric pressure. Moreover, and for both flow regime situations, there is a conduit diameter which maximizes the vent pressure, whereas the atmospheric pressure limits this pressure and therefore the conduit diameter (Figures 5a and 6a). The effect of magma reservoir pressure P_0 is particularly significant,

since a larger pressure produces larger vent pressures for the same conduit diameter and larger conduit diameters for a fixed vent pressure (Figure 5a), while displaying an opposite trend in the gas and magma velocities at the vent (Figures 5b-5d). The PCA flow regime and magma reservoir pressure P_0 also produce similar vent pressure and gas and magma velocity distributions with the conduit diameter (Figures 6a-6d). In this case, however, there is a much more pronounced velocity disequilibrium between the phases which increases with a decrease of P_0. In particular, a vent pressure of about 0.6 MPa corresponds to an overpressure at the vent created by a lava pond in the crater which is about 20 m deep. This produces BF conduit diameters of about 25 m for P_0=181 MPa and 110 m for P_0=197.2 MPa, and PCA conduit diameters of about 30 m for P_0=181 MPa and 90 m for P_0=197.2 MPa. The simulation results pertaining to the GL flow regime are similar to phase II of the 1989 eruption (since the mass eruption rates of these phases are similar) and are discussed below.

Phase II activity of the 1989 eruption from September 27 to October 9 which produced strombolian explosions, lava fountains, and lava flows in Valle del Leone was simulated by all three models of magma ascent discussed above and for different magma reservoir pressures.

PCA results which depict the variation of vent pressure and gas and magma velocities with the conduit diameter for phase II are similar to those shown in Figure 6 for phase Ib, except that the smaller mass eruption rate of this phase produces lower choked conduit diameters (D=3.8 m for P_0=197.2 MPa, and D=6.7 m for P_0=181 MPa, as opposed to D=7.1 and D=11.8 m, respectively). Cases 9 and 10 in Table 3 summarize the choked flow parameters of these simulations. It is also important to note that a low magma reservoir pressure (case 10) produces a choked flow conduit exit pressure which is less than the atmospheric and is therefore not consistent with the activity as further discussed below. Moreover, the simulations produced gas volumetric fractions at the vent which are less than about 0.74.

Phase II activity of the 1989 eruption was also simulated with gas loss to fractures involving different permeabilities of the surrounding conduit rocks . The results from cases 11-13 in Table 3 for a conduit diameter of 5 m are shown in Figures 7-9. Figure 7 shows magma pressure and gas volumetric fraction variations along the conduit corresponding to a large permeability of 10^{-8} m^2 and represents an underdamped gas volumetric fraction behavior, Figure 8 corresponds to a much smaller permeability of 10^{-12} m^2 and represents a critically damped behavior of gas fraction, whereas Figure 9 corresponds to the permeability of 10^{-13} m^2 and to an overdamped behavior of the gas volumetric fraction along the conduit. (Underdamping, critical damping, and overdamping are terms which are used to represent a system's dynamical response owing to a viscous damping force which is proportional to the system's velocity.) Notice in Figures 7-9 that there is a rapid drop of the gas volumetric fraction when the magma pressure exceeds the local lithostatic pressure and that very small variations of magma pressure above lithostatic produce very large variations of the gas volumetric fraction for large rock permeabilities. For all permeabilities, the gas loss to fractures is very efficient but requires greater magmatic pressures than lithostatic as the rock permeability

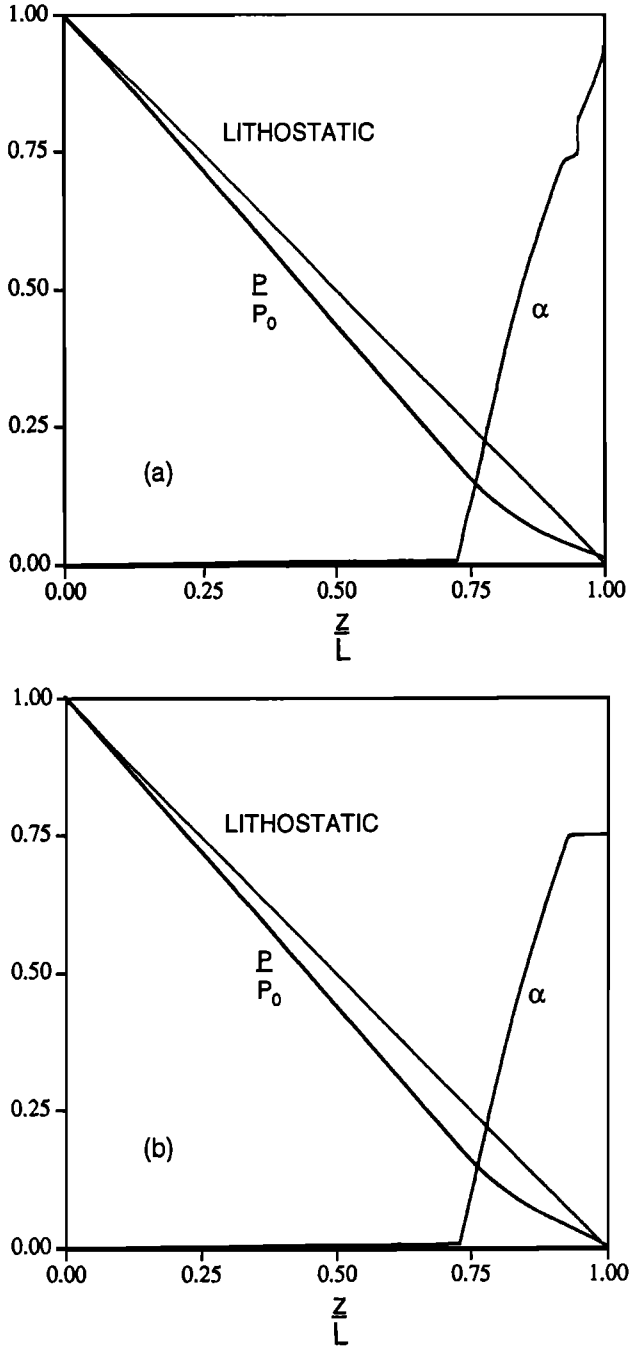

Figure 4. Nondimensional pressure and gas volumetric fraction variations along the conduit corresponding to cases 5 and 6 in Table 3 (phase Ib of the 1989 eruption). (a) The choked BF and (b) the choked PCA flow. Notice that the former flow regimes produce larger conduit exit pressure and gas volumetric fraction than the latter flow regimes.

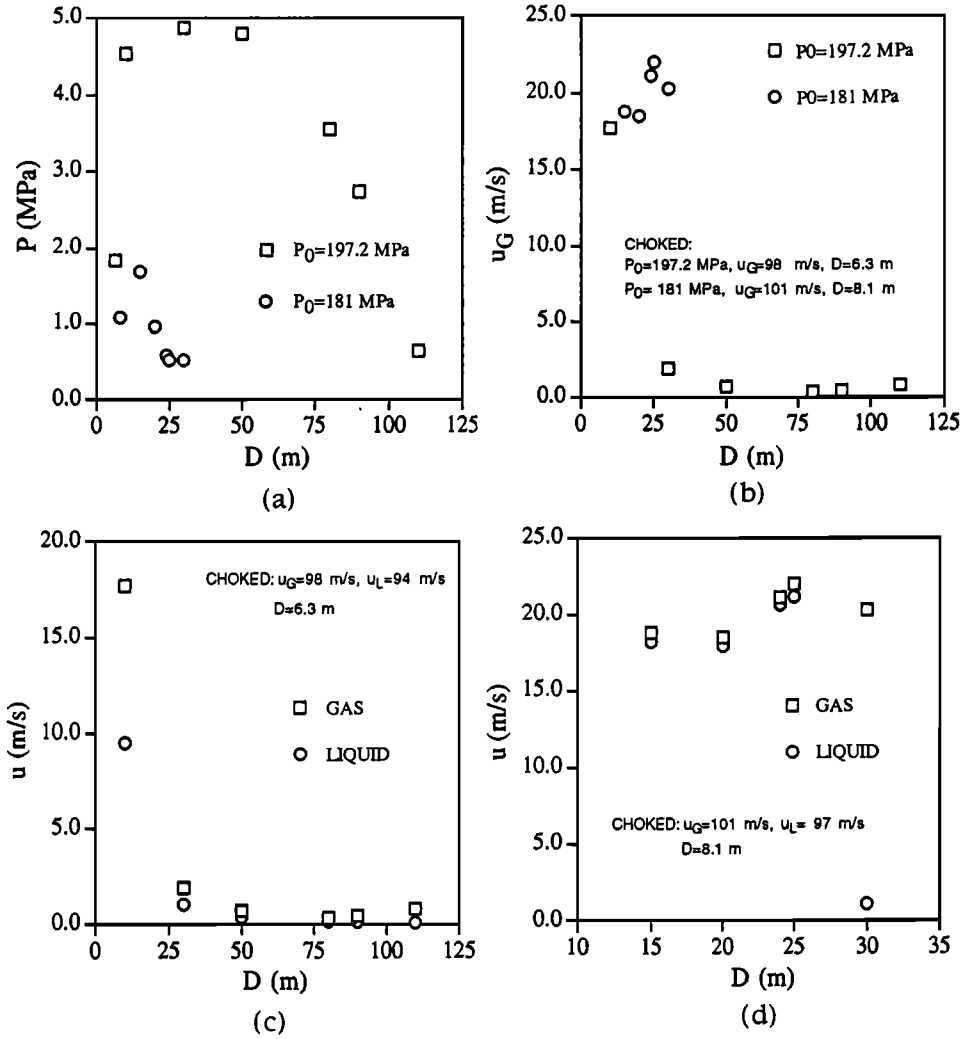

Figure 5. Variation of vent pressure and gas and magma velocities with the conduit diameter and magma reservoir pressure for BF flow regimes (phase Ib of the 1989 eruption). (a) Vent pressure variation with conduit diameter for different P_0, (b) vent gas velocity variation with conduit diameter for different P_0, (c) gas and magma velocity variations with conduit diameter for P_0=197.2 MPa, and (d) gas and magma velocity variations with conduit diameter for P_0=181 MPa. Notice that a 20-m-deep lava pond limits the vent pressure to about 0.6 MPa.

decreases. Case 14 results corresponding to a conduit diameter of 10 m and permeability of 10^{-8} m^2 produce a similar gas volumetric fraction behavior as in case 11. It is important to note in Figures 7-9 that the rock permeability decreases from 10^{-8} to 10^{-13} m^2 produce vent pressure increases from atmospheric to 4.8 MPa but that this does not affect the gas volumetric fractions at the vent which remain at about 0.25. The magma reservoir pressure of 181 MPa and 10 m conduit diameter display gas volumetric fraction trends with the rock permeability which are similar to those corresponding to P_0=197.2 MPa and are not reported in the paper.

The phase I and II activities of the eccentric 1974 eruption were simulated by all three fluid dynamic models of magma ascent by accounting for an inclined conduit diameter at 45° and the same conduit lengths as those of the 1989 eruption.

Simulation results of phase I pertaining to pressure and gas volumetric fraction distributions along the conduit for the BF and PCA flow regimes are shown in Figure 10 and are indicated as cases 15 and 16 in Table 3. The BF simulation produces a choked conduit diameter of about 1 m, and vent gas and magma velocities of about 90 m/s, a gas volumetric fraction of 0.97, and a pressure of about 1 MPa. The corresponding values of these parameters for the PCA flow are: $D \approx 2$ m, $u_G \approx 250$ m/s, $u_L \approx 10$ m/s, $\alpha \approx 0.7$, and $P \approx 0.2$ MPa.

Bubbly-particle/droplet and bubbly-churn turbulent-annular flow simulations of phase II of the 1974 eruption are represented by cases 17 and 18 in Table 3. These simulations produce similar vent conditions but slightly lower values of conduit diameters and vent pressures in comparison to cases 15 and 16 which have a larger mass eruption rate. The results of simulations involving gas loss to fractures (cases 19-23 in Table 3) are illustrated in Figures 11 and 12 and do not produce underdamped volumetric fraction behavior as illustrated in Figure 7 for a vertical conduit system. Cases 19-21

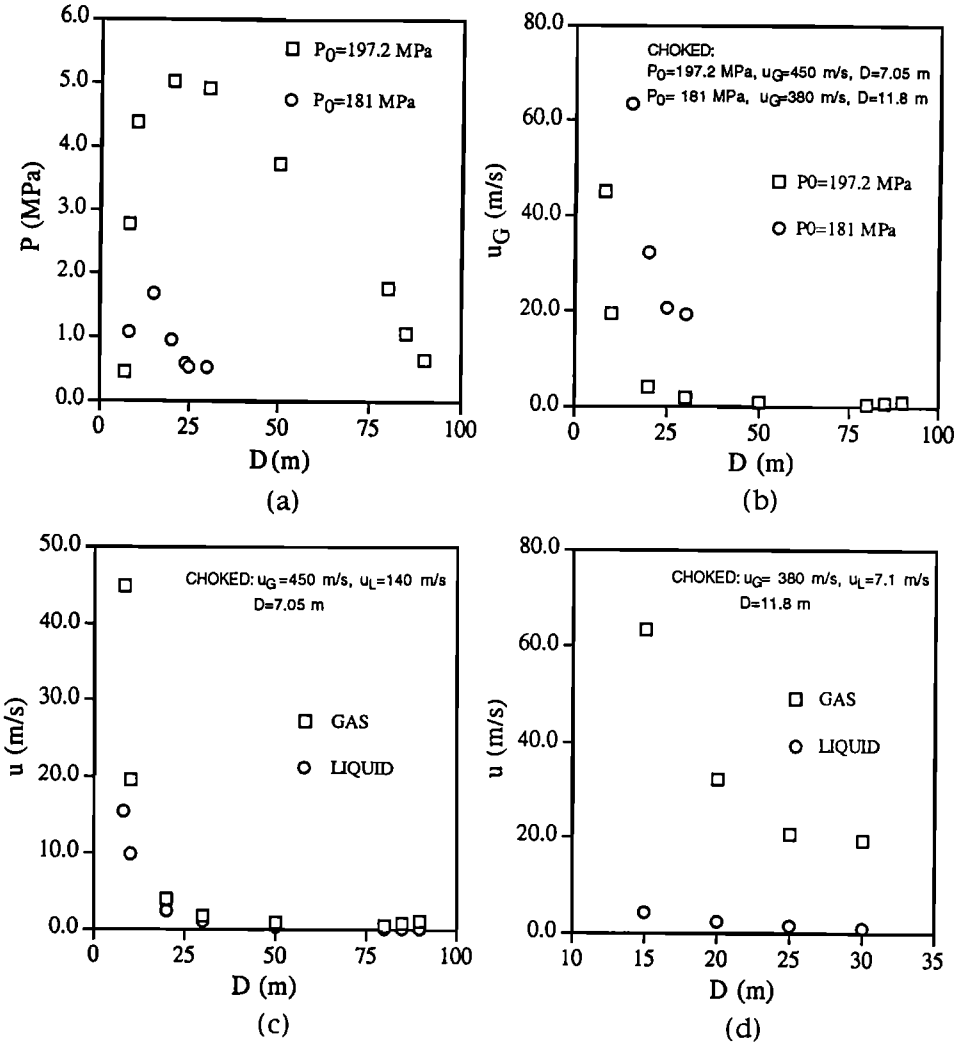

Figure 6. Variation of vent pressure and gas and magma velocities with the conduit diameter and magma reservoir pressure for PCA flow regimes (phase Ib of the 1989 eruption). (a) Vent pressure variation with conduit diameter for different P_0, (b) vent gas velocity variation with conduit diameter for different P_0, (c) gas and magma velocity variations with conduit diameter for P_0=197.2 MPa, and (d) gas and magma velocity variations with conduit diameter for P_0=181 MPa. Notice that a 20-m-deep lava pond limits the vent pressure to about 0.6 MPa.

show progressively higher vent gas volumetric fractions (α=0-0.1) and pressures (P=1.2-3.1 MPa) and only the latter simulation shows a substantial critical damping of the gas fraction (Figure 12a). Decreasing the rock permeability to 10^{-14} m^2 (case 22 in Table 3) produces a gas volumetric fraction at the vent of about 0.5 and pressure of about 23 MPa (Figure 12b). An increase in the conduit diameter to 10 m (case 23 in Table 3) produces a degassed magma (similar to case 19) and a vent pressure of about 2 MPa which is about 70% larger than for case 19. As further discussed below, different behavior of flow parameters corresponding to vertical and inclined conduits is caused by a higher lithostatic pressure acting on magma which flows through an inclined conduit.

Discussion

The paroxysmal event on September 13, 1989 (phase Ia), which produced a high wall of lava occupying the entire South-East Crater and magma fragmentation implies the existence of PCA flow regimes during lava fountaining which subsequently changed into BF flow regimes as the magma fragmentation surface moved downward. PCA magma ascent results (case 3) with its associated high gas and magma velocities at the vent (about 500 and 45 m/s, respectively) are consistent with the intense lava fountaining activity during the morning of September 13 and observations that a wall of lava formed above the crater. The lava fountaining and paroxysmal events also imply the issuance of a high-

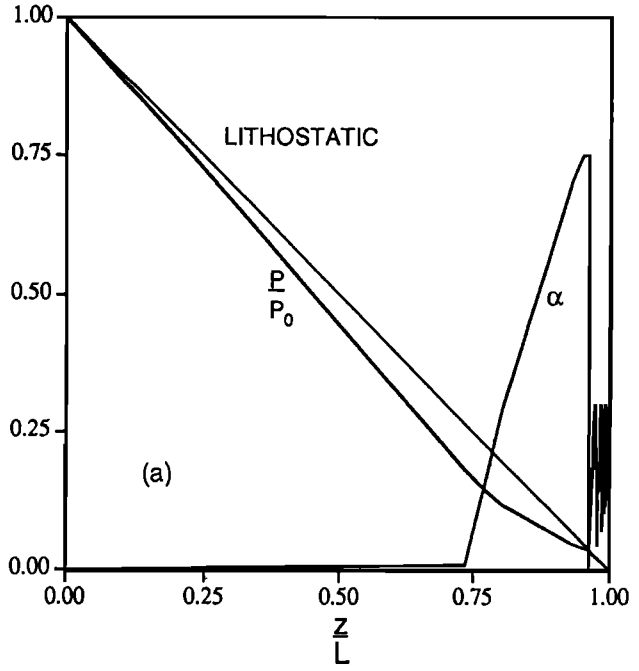

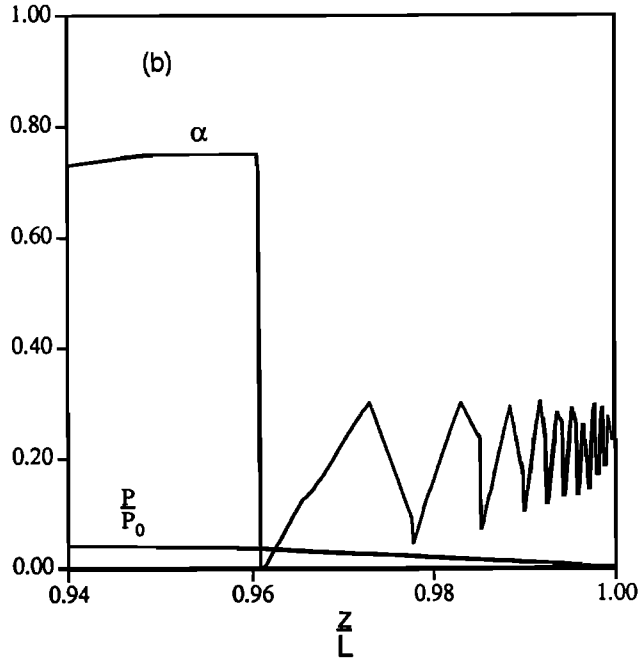

Figure 7. Pressure and gas volumetric fraction variations along the conduit with gas loss to fractures (case 11 in Table 3) (phase II of the 1989 eruption). A high rock permeability of 10^{-8} m^2 produces an underdamped and low gas volumetric fraction at the vent. Notice that slight magma pressure increases above lithostatic are very efficient for releasing gas to fractures and that the magma pressure follows the lithostatic pressure very closely in the upper regions of the conduit. Figure 7b illustrates the behavior of pressure and gas volumetric fraction oscillations close to the conduit exit.

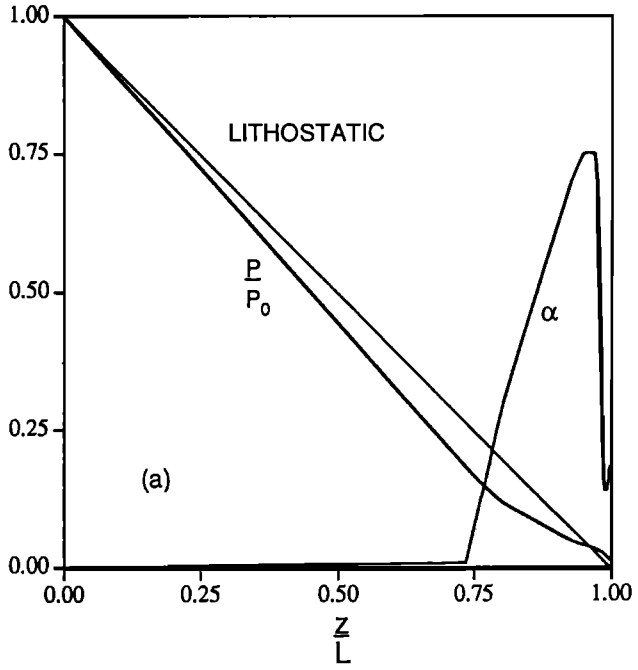

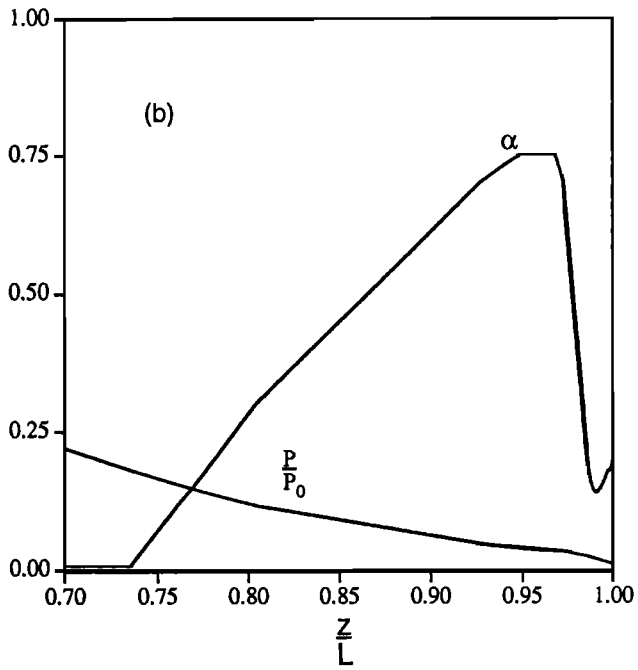

Figure 8. Pressure and gas volumetric fraction variations along the conduit with gas loss to fractures (case 12 in Table 3) (phase II of the 1989 eruption). A low rock permeability of 10^{-12} m^2 produces a critically damped and low gas volumetric fraction at the vent. Notice that magma pressure increases above lithostatic are required for efficient release of gas to fractures. Figure 8b illustrates the behavior of pressure and gas volumetric fraction in the upper portion of the conduit.

pressure jet of gas and magma at the vent which suggests the existence of a choked flow condition at the conduit exit as assumed in the simulations (cases 1-3). The onset of internal collapses within the volcanic system following the paroxysmal event suggests that either the magma supply into the system was terminated or that there were inward conduit wall collapses within the volcanic system. The latter situation is clearly consistent with magma ascent simulations which predicted considerable differences between the lithostatic and magmatic pressures (less than about 25 MPa) over a significant portion of the conduit (1-4 km below the summit). These large pressure differences are sufficient to cause rock fracturing which may consequently produce melting of some of these rocks and form a secondary magma reservoir within a shallow part of the volcanic system. This hypothesis finds a justification by the presence of a stratigraphic discontinuity between the volcanic and sedimentary covers and from the existence of pyroclastic layers above this structure [*Chester et al.*, 1985] which may easily fracture, either induced by magma ascent and/or tectonic tensile stresses. Moreover, the seismic activity before and during the opening of the 1989 fracture system was interpreted as being localized from 3 to 5 km below the summit [*Barberi et al.*, 1990]. The predicted conduit diameters of about 20 m representing phase Ia activity should be viewed as the maximum conduit diameter produced by the 1989 eruption, since this diameter corresponds to the maximum mass eruption rate during the eruption. The opening of eruptive fractures from the South-East Crater at the beginning of phase Ib of the 1989 eruption may had been caused by the magma overpressure in the upper portions of the conduit as predicted by the simulations and shown in Figure 3.

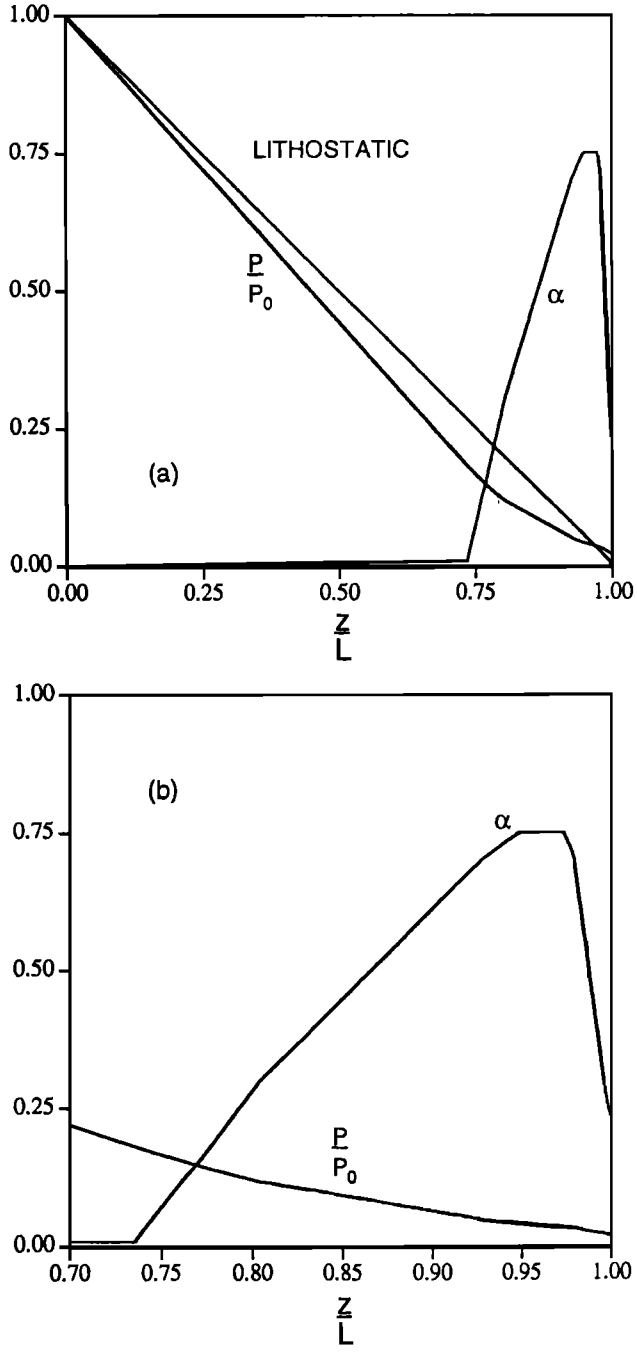

Figure 9. Pressure and gas volumetric fraction variations along the conduit with gas loss to fractures (case 13 in Table 3) (phase II of the 1989 eruption). A rock permeability of 10^{-13} m^2 produces an overdamped and low gas volumetric fraction at the vent. Notice that considerable magma pressure increases above lithostatic are required for releasing gas to fractures, and that the vent pressure becomes considerably greater than the atmospheric. Figure 9b illustrates the behavior of pressure and gas volumetric fraction in the upper portion of the conduit.

The mixed strombolian, lava fountaining, and lava overflow from the South-East Crater during phase Ib of the 1989 eruption may be explained by BF, PCA, and GL magma ascent models. The strombolian and lava fountaining activity is consistent with the choked PCA simulation, since it produces large vent pressure and gas and magma velocities (Figure 6), and nonfragmented magma in the annular flow regime. The BF simulation (case 5) produces too high vent gas volumetric fraction and magma fragmentation within the conduit which is not consistent with the early phase Ib strombolian and lava fountaining activity. To explain the lava overflow activity from the South-East Crater with one of the considered magma ascent models, it is necessary to take into account the pressure created at the vent by the lava pond and the observational data. For a 20-m-deep pond, this pressure is about 0.6 MPa and must involve low gas volumetric fractions at the vent. Based on these considerations, the BF simulation represented by case 7 (P_0=181 MPa) should be eliminated, since magma fragments within the conduit and produces a high gas volumetric fraction at the vent ($\alpha \approx 0.94$). BF and PCA flow simulations corresponding to P_0=197.2 MPa (nonchoked cases 5 and 6 in Table 3) produce conduit diameters in excess of 100 m which are considerably larger than the maximum predicted conduit diameter of about 20 m corresponding to the maximum mass eruption rate during phase Ia and should also be eliminated. The lava overflow activity

of phase Ib can be explained, however, by the GL flow regimes, whereby the gas loss to surrounding conduit fractures produces low gas volumetric fractions at the vent and vent pressures depending on the fracture permeability, as further discussed below for phase II of the 1989 eruption. In effect, the average of phase Ib activity is consistent with the PCA and GL flow regimes which may have been established during the eruption by the combined effects of magma ascent and by the corresponding internal volcanic system response.

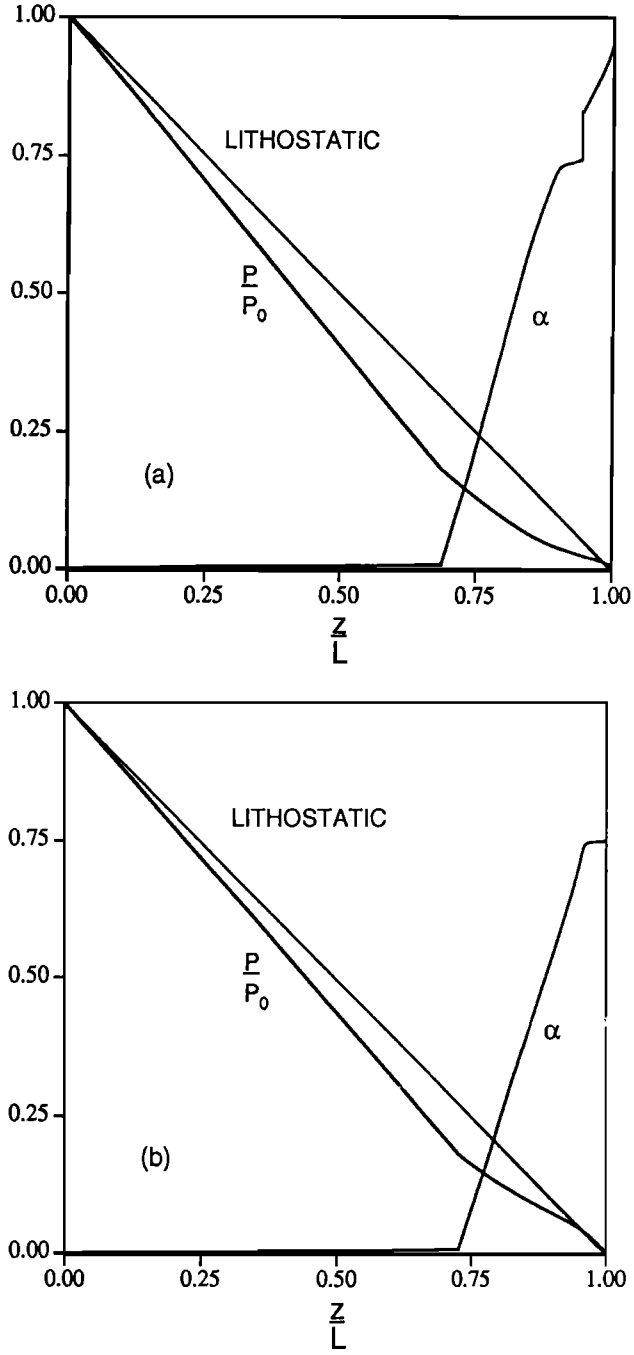

Figure 10. Nondimensional pressure and gas volumetric fraction variations along the conduit corresponding to cases 15 and 16 in Table 3 (phase I of the 1974 eruption). (a) BF and (b) PCA flow regimes. Notice that BF flow regimes produce larger conduit exit pressure and gas volumetric fraction than PCA flow regimes.

The eruption of degassed lava flows in Valle del Leone and Valle del Bove during phase II of the 1989 eruption can be simulated most effectively by a magma ascent model which accounts for the gas loss to fractures. The results of these simulations are shown in Figures 7-9 and are represented by cases 11-14 in Table 3 for different fracture permeabilities. As noted above, the effect of decreasing the surrounding conduit rock permeability is to increase the pressure at the vent while maintaining an efficient release of gas to fractures. In particular, a high rock fracturing near the conduit exit may be very efficient not only to produce gas loss from magma but also to produce large gas volumetric fraction variations in this region as the magma pressure in the conduit attempts to follow the local lithostatic pressure. It should be noted, however, that the pronounced gas volumetric fraction oscillations near the conduit exit predicted by the model for the rock permeability of 10^{-8} m^2 (Figure 7) should be difficult to realize in practice due to a finite time for the released gas to flow out of the volcanic system which is not accounted for by the model. As a consequence, the weak strombolian and degassed lava flow activity during phase II of the 1989 eruption can be explained by the changing permeability of the system during this eruption phase, where this permeability may have been controlled by the overpressure created by magma flowing in the conduit and by the rate of gas release from the volcanic system to the atmosphere through different craters and vents. The predicted conduit diameter of about 5 m for phase II suggests maximum dimension of a subvertical conduit related to eruptive fissures with lava flows.

The eccentric phase I of the 1974 eruption produced strong strombolian, lava fountaining, and lava flow activity and was simulated by the choked BF and PCA flow regimes. The results from these simulations give a conduit diameter which is less than 2 m and vent velocities, gas volumetric fractions, and pressures necessary to produce the observed activity. The PCA flow simulation results (case 16 in Table 3) are, however, more consistent with the field data than the BF results, since the latter produce magma fragmentation in the conduit which does not appear to be consistent with the absence of an eruptive column of gas and ash.

The strombolian and effusive lava flow activity during phase II of the 1974 eruption is consistent with PCA and GL simulations. The lithostatic pressure of this eruption acting on magma flowing in a conduit is higher than for a vertical conduit system because in an inclined conduit a lithostatic pressure is produced by a greater body force than that acting on magma. This produces higher vent pressures and very low volumetric fractions for high-permeability rocks and implies that the effusive eruptions from eccentric eruptions of Etna should on the average dominate over the explosive ones which is generally considered the case [*Chester et al.*, 1985].

Based on the magma ascent simulations of different phases of the 1989 and 1974 eruptions at Etna, it can be

hypothesized that the eruptive activity of this volcano is related to the magma conditions at the source and characteristics of the volcanic edifice. These simulations, together with geophysical and geological data [*Lentini*, 1981; *Chester et al.*, 1985; *Hirn et al.*, 1991], suggest the existence of a magma storage zone from 8 to 9 km below the summit. At about 1-4 km below the summit, the magma may accumulate among the fractured rocks created by the internal conduit wall collapses as produced by the previous magma ascents which created magma pressures below the local lithostatic pressure. Such a modeling prediction is consistent with the existence of shallow earthquakes at about 2 km depth which had been registered before recent eruptions [*Lo Giudice and Rasà*, 1992] and thus implies the existence of a structurally weak region of the system at this depth. Based on simulations, it is also reasonable to assume that the magma at Etna during intereruptive cycles is degassing at depths from 2 to 5 km below the summit and that eruptions take place when the gas pressure builds up, causing rock fracturing in the upper regions of the volcanic system. For a highly fractured system, such pressure increases may occur at different locations within the system and thus produce variable volcanic activity at different locations even during a single eruption.

The opening of vents and extensive degassing at the central craters of Etna suggest the existence of structurally weak regions below these craters whose permeabilities change during the coarse of an eruption. During the initial phase of an eruption, such a condition of the system may produce mixed strombolian and lava fountaining activity due to the overpressure of magma within the upper regions of the system as it relaxes by releasing gas to the atmosphere and opens new fractures which may shift magma ascent along different paths. The existence of BF, PCA, or GL flow regimes within the conduits can then be associated with the internal system constraints (such as the compressive and tensile tectonic stresses) which limit flow dimensions, magma overpressures required to fracture rocks, and gas loss to fractures. For a volcano such as Etna with small mass eruption rates, the gas loss to fractures affects dramatically the nature of the erupting magma and explains the eruption of degassed lava during later stages of an eruption when the ascending magma encounters a sufficient fracturing of the system.

The 1989 and 1974 eruptions of Etna represent two limiting cases of the eruptions of this volcano where the former may represent those eruptions caused by magma ascent along the central conduit. The four summit craters of Etna may be considered as four distinct vents emanating from or being connected by a shallow part of the central system, where the eruptive activity of two opposite cones (North-East and South-East) is due to local tensile stress variations in recent times. The magma column level at the end of the 1989 eruption and possible partial or total conduit closures at different depths within 2 km of the summit may explain the formations of fissure and/or flank eruptions near the summit region. The 1974 eruption may be, however, considered representative of those eruptions caused by magma ascent along paths which are connected with the central conduit only at large depths and caused by movements of tectonic structures which give rise to intense seismic activity before the eruptions [*Bottari et*

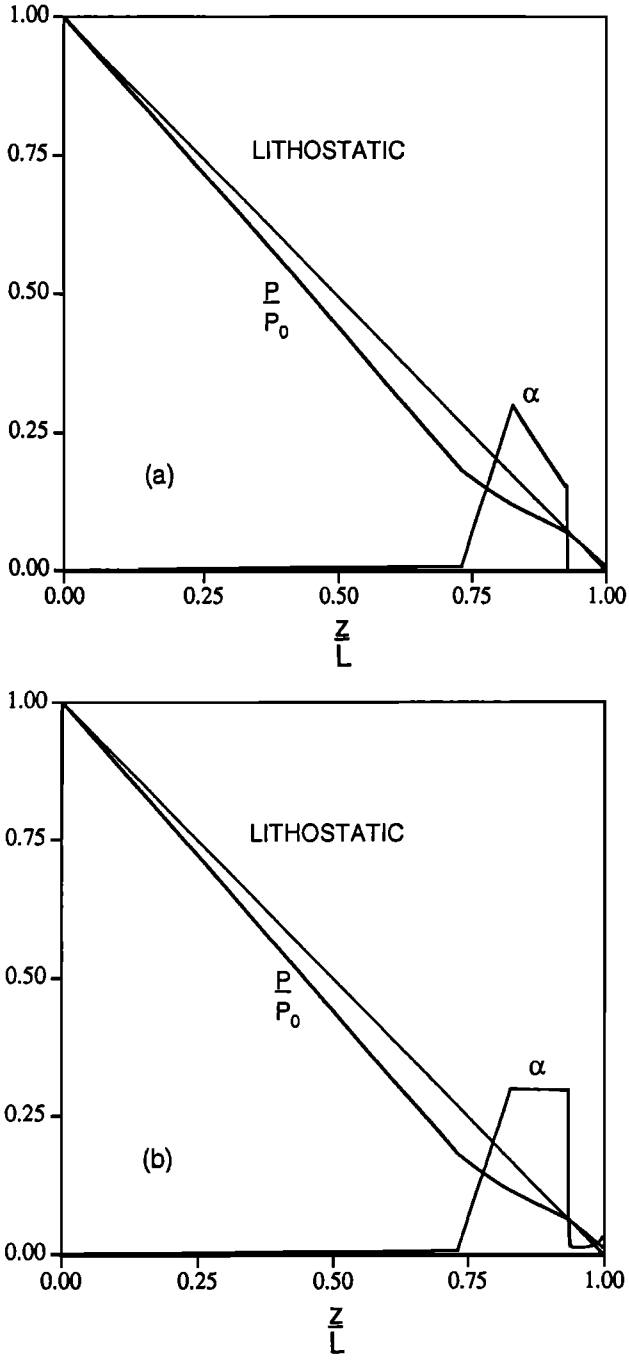

Figure 11. Pressure and gas volumetric fraction variations along the conduit with gas loss to fractures (cases 19-20 in Table 3) (phase II of the 1974 eruption). The corresponding rock permeabilities of (a) 10^{-9} m^2 and (b) 10^{-12} m^2 produce overdamped and very low gas volumetric fractions at the vent. Notice that magma pressure increases above lithostatic are required for releasing gas to fractures and that the vent pressure becomes considerably greater than the atmospheric.

al., 1976]. In recent times, these types of eruptions appear to be statistically less dominant than the 1989-like eruptions.

Summary and Conclusions

A nonequilibrium, isothermal, and two-phase flow model of magma ascent in volcanic conduits was employed to study different eruptive phases of 1989 and 1974 eruptions of Etna. The model accounts for bubbly-particle/droplet flow with magma fragmentation, bubbly-churn turbulent-annular flow without magma fragmentation, as well as for the gas loss from the conduit to fractures when the magma pressure exceeds the local lithostatic pressure. Simulations were carried out for different conduit lengths, magma reservoir pressures, crystal volumetric fractions, magma temperatures, and different flow regimes for different eruptive phases of the 1989 and 1974 eruptions.

Phase Ia of the 1989 eruption produced high lava fountains and an eruptive column of gas and ash which was simulated with magma ascent models which allow for bubbly and churn turbulent-annular flow and magma fragmentation. This produced a conduit diameter of about 20 m with a conduit length of 8.3 km below the summit. The mixed strombolian, lava fountaining, and lava overflow activity from the South-East Crater of phase Ib of the 1989 eruption was found to be consistent with the bubbly-churn turbulent-annular flow model which produced a conduit diameter of 6-8 m. This range of conduit diameters for phase I activity may be associated with the changing stress levels within the volcanic edifice as magma channeled its way toward the surface. The degassed lava flow activity of phase II of the 1989 eruption was found to be consistent with a magma ascent model which accounts for gas loss to fractures. The results from modeling indicate the importance of the surrounding rock permeabilities which may produce underdamped, critically damped, or overdamped gas volumetric fraction behavior in the conduit after the magma pressure exceeds the local lithostatic pressure. The pyroclastic and lava flow activity of phase I of the 1974 eruption was simulated with bubbly-gas particle/droplet and bubbly-churn turbulent-annular flow regimes which produced a conduit diameter of about 2 m. Phase II of the same eruption was simulated with gas loss to fractures, and the results did not produce underdamped gas volumetric fraction behavior as in the vertical conduit case.

Magma ascent simulations of different phases of 1989 and 1974 eruptions suggest the existence of a magma reservoir at about 8-9 km below the summit and of a structurally weak zone from 1 to 4 km below the summit where magma may reside within a mushy region during intereruptive cycles of the volcano. Simulation results also suggest that during the initial stages of eruptions of Etna when magma produces pathways to the surface, the magma overpressure in the upper regions of conduits may significantly weaken the structures in these regions and produce new eruptive fractures. The subsequently ascending magma may effectively degas into these fractures and produce eccentric degassed lava flow activity with gas venting from central craters. The 1989 and 1974 eruptions of Etna represent two limiting erup-

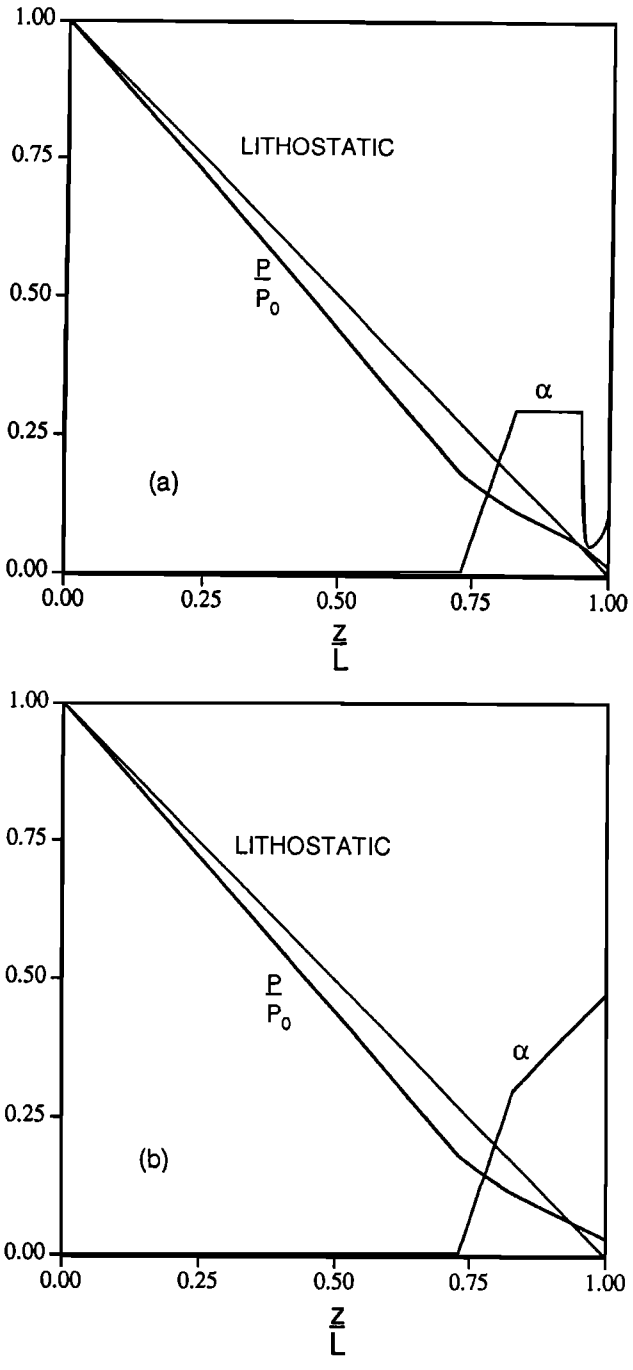

Figure 12. Pressure and gas volumetric fraction variations along the conduit with gas loss to fractures (cases 21-22 in Table 3) (phase II of the 1974 eruption). (a) A rock permeability of 10^{-13} m^2 produces critically damped and low (about 0.1) gas volumetric fraction at the vent, whereas (b) a permeability of 10^{-14} m^2 produces no efficient gas loss to fractures and a gas volumetric fraction of about 0.5. The vent pressures are considerably greater than the atmospheric.

tions, whereby the former was found to be consistent with magma ascent along a central conduit and the latter along an inclined conduit which connects to the central conduit at a large depth. The effectiveness of gas loss from the central and inclined conduits depends strongly on the surrounding rock permeabilities and on the local lithostatic pressure which for the inclined conduit of the 1974 eruption is larger and appears to diminish the gas volumetric fraction oscillations during magma ascent.

Internal fracture and tectonic stress characteristics of the volcanic system of Etna appear to play a significant role in establishing eruptive activity, since these characteristics can determine different flow regimes, the quantity of gas being lost from conduits to fractures, and the conduit dimensions during magma ascent. These internal system characteristics, together with the characteristics of the magma and of its storage region(s), should be considered as major factors which control the intensity and nature of different styles of activity (pyroclastic, strombolian, lava fountaining, lava overflow from craters, lava effusion from fractures). To physically model the changes of this activity during an eruption requires the establishment of high-quality geophysical and volcanological data aimed at the internal system definition of Etna.

Notation

A	flow cross-sectional area.
d	particle diameter.
D	conduit diameter.
f	friction coefficient.
F	drag force.
g	gravitational acceleration.
G	mass flow rate per unit area.
K	conduit entrance loss coefficient.
K'	permeability.
L	conduit length.
M	mass effusion rate.
P	pressure.
q	mass lost to fractures
Re	Reynolds number.
T	temperature.
u	velocity.
X	exsolved gas mass fraction.
Y	dissolved gas mass fraction in magma.
z	distance along the conduit.

Greek

α	gas volumetric fraction.
ρ	density.
θ	inclination angle of the conduit.
ϕ	crystal volumetric fraction.
μ	viscosity.

Subscripts

atm	pertaining to the atmosphere.
b	bubbly flow.
c	country rock.
f	fragmentation.
G	gas phase.
Gd	gas dissolved.
l	lithostatic.
L	liquid phase or magma.
o	magma reservoir location.
p	particles or pyroclasts phase.
s	exsolution.
w	conduit wall.

Acknowledgments. This research was supported in part by the Commission of the European Communities, DGXII, Environment Programme, Climatology and Natural Hazards Unit, in the framework of contract EV5V-CT92-0190. We also wish to thank S. Calvari and M. Coltelli for useful discussions regarding the field data.

References

Allard, P., et al., Eruptive and diffusive emissions of CO_2 from Mount Etna, *Nature, 351*, 387-391, 1991.

Allard, P., Etna's volatiles, mid-term progress report on CEC contract EV5V-CT92-0177, European Commission, Brussels, Belgium, May 1994.

Armienti, P., R. Clocchiatti, F. Innocenti, B. Marty, N. Metrich, M. Mosbah, M.T. Pareschi, and M. Pompilio, Abundance, behaviour and sources of volatiles in Mt. Etna Magma, paper presented at the International Workshop on European Laboratory Volcanoes, Aci Castello (Catania, Italy), European Commission, Brussels, Belgium, June 18-21 1994a.

Armienti, P., M.T. Pareschi, F. Innocenti, and M. Pompilio, Effects of magma storage and ascent on the kinetics of crystal growth, *Contrib. Mineral. Petrol., 115*, 402-414, 1994b.

Barberi, F., A. Bertagnini, and P. Landi (Eds.), *Mt. Etna: The 1989 Eruption*, Giardini, Pisa, Italy, 1990.

Bertagnini, A., S. Calvari, M. Coltelli, P. Landi, M. Pompilio, and V. Scribano, L'eruzione dell'Etna del settembre-ottobre 1989, *Boll. GNV, 2*, 669-681, 1989.

Bottari, A., E. Lo Giudice, G. Patanè, R. Romano, and C. Sturiale, L'eruzione del gennaio-marzo 1974, *Riv. Min. Sicil., 154-156*, 175-199, 1976.

Calvari, S., M. Coltelli, M. Pompilio, and V. Scribano, Analysis of three strong explosive episodes in recent activity at Mt. Etna volcano (Italy), *Eos. Trans. AGU, 72* (44), Fall Meet. Suppl., 561, 1991.

Chester, D.K., A.M. Duncan, J.E. Guest, and C. Kilburn, *Mount Etna: The Anatomy of a Volcano*, 404 pp., Chapman and Hall, New York, 1985.

Coniglio, S., and F. Dobran, Simulations of magma ascent and pyroclast dispersal at Vulcano (Aeolian Islands, Italy), *J. Volcanol. Geotherm. Res., 65*, 297-317, 1995.

Dobran, F., Nonequilibrium modeling of two-phase critical flows in tubes, *J. Heat Transfer, 109*, 731-738, 1987.

Dobran, F., Nonequilibrium flow in volcanic conduits and application to the eruptions of Mt. St. Helens on May 18, 1980, and Vesuvius in AD 79, *J. Volcanol. Geotherm. Res., 49*, 285-311, 1992.

Dobran, F., CONDUIT2M-Computer programs for modeling steady-state two-phase flows in volcanic conduits with different flow regimes and gas loss to fractures, Global Volcanic and Environ. Syst. Simul., Report, Rome, 1994.

Dobran, F., *Etna: Magma and Lava Flow Modeling and Volcanic System Definition Aimed at Hazard Assessment*, 277 pp., Tipografia Massarosa Offset, Massarosa, Italy, 1995.

Dobran, F., and P. Papale, CONDUIT2-A computer program for modeling steady-state two-phase flows in volcanic conduits, *VSG Rep. 92-5*, Giardini, Pisa, Italy, 1992.

Fabbri, A., S. Rossi, R. Sartori, and A. Barone, Evoluzione neogenica dei margini marini dell'Arco Calabro-Peloritano: Implicazioni geodinamiche, *Mem. Soc. Geol. It., 24*, 357-366, 1982.

Frazzetta, G., and L. Villari, The feeding of the eruptive activity of Etna volcano: The regional stress field as a constraint to magma uprising and eruption, *Bull. Volcanol., 44*, 269-282, 1981.

Grindley, G.W., Structural control of volcanism at Mount Etna, *Philos. Trans. R. Soc. London A, 274*, 165-175, 1973.

Guest, J.E., A.T. Huntington, G. Wadge, J.L. Brander, B. Booth, S. Carter, and A. Duncan, Recent eruption of Mount Etna, *Nature, 250*, 385-387, 1974.

Heiken, G., K. Wohletz, and J. Eichelberger, Fracture filling and intrusive pyroclasts, Inyo Domes, California, *J. Geophys. Res., 93*, 4335-4350, 1988.

Hirn, A., A. Nercessian, M. Sapin, F. Ferrucci, and G. Wittlinger, Seismic heterogeneity of Mt Etna: Structure and activity, *Geophys. J. Int., 105*, 139- 153, 1991.

Hughes, J.W., J.E. Guest, and A.M. Duncan, Changing styles of effusive eruption on Mount Etna since AD 1600, in *Magma Transport and Storage*, edited by M.P. Ryan, pp. 385-406, John Wiley, New York, 1990.

Jaupart, C., and C.J. Allègre, Gas content, eruption rate and instabilities of eruption regime in silicic volcanoes, *Earth Planet. Sci. Lett., 102*, 413-429, 1991.

Kuntz, M.A., P.D. Rowley, N.S. Macleod, R.L Reynolds, L.A. McBroome, A.M. Kaplan, and D.J. Lidke, Petrography and particle-size distribution of pyroclastic-flow, ash-cloud, and surge deposits, *U.S. Geol. Surv. Prof. Pap., 1250*, 525-539, 1981.

Lentini, F., The geology of the Mt. Etna basement, *Mem. Soc. Geol. It., 23*, 7-25, 1981.

Lo Giudice, E., G. Patanè, R. Rasà, and R. Romano, The structural framework of Mt. Etna, *Mem. Soc. Geol. It., 23*, 125-158, 1982.

Lo Giudice, E., and R. Rasà, Very shallow earthquakes and brittle deformation in active volcanic areas: The Etnean region as an example, *Tectonophysics, 202*, 257-268, 1992.

Metrich, N., and R. Clocchiatti, Melt inclusion investigation of the volatile behaviour in historic alkali basaltic magmas of Etna, *Bull. Volcanol., 51*, 185- 198, 1989.

Murray, J.B., High-level magma transport at Mount Etna volcano, as deduced from ground deformation measurements, in *Magma Transport and Storage*, edited by M.P. Ryan, pp. 357-383, John Wiley, New York, 1990.

Papale, P., and F. Dobran, Modeling of the ascent of magma during the Plinian eruption of Vesuvius in AD 79, *J. Volcanol. Geotherm. Res., 58*, 101-132, 1993.

Papale, P., and F. Dobran, Magma flow along the volcanic conduit during the Plinian and pyroclastic flow phases of the May 18, 1980, Mount St. Helens eruption, *J. Geophys. Res., 99*, 4355-4373, 1994.

Pinkerton, H., and R.S.J. Sparks, The 1975 subterminal lavas, Mount Etna: A case history of the formation of a compound lava field, *J. Volcanol. Geotherm. Res., 1*, 167-182, 1976.

Rittmann, A., Structure and evolution of Mount Etna, *Philos. Trans. R. Soc. London, A 274*, 5-16, 1973.

Tanguy, J.C., Les eruption historiques de l'Etna: Chronologie et localisation, *Bull. Volcanol., 44*, 585-640, 1981.

Touloukian, Y.S., W.R. Judd, and R.F. Roy, *Physical Properties of Rocks and Minerals*, McGraw-Hill, New York, 1981.

Trigila, R., F.J. Spera, and C. Aurisicchio, The 1983 Mount Etna eruption: Thermochemical and dynamical inferences, *Contrib. Mineral Petrol., 104*, 594-608, 1990.

Vergniolle, S., and C. Jaupart, Dynamics of degassing at Kilauea, Hawaii, *J. Geophys. Res., 95*, 2793-2809, 1990.

Wallis, G.B., *One-Dimensional Two-Phase Flow*, McGraw-Hill, New York, 1969.

Woods, A.W., and T. Koyaguchi, Transitions between explosive and effusive eruptions of silicic magmas, *Nature, 370*, 641-644, 1994.

F. Dobran and S. Coniglio, Global Volcanic and Environmental Systems Simulation, Via Caio Mario 27, 00192 Rome, Italy. (e-mail: f.dobran@agora.stm.it)

(Received October 24, 1994; revised July 10, 1995; accepted July 21, 1995.)